Perfusion CT of the Brain and Liver and of Lung Tumors: Use of Monte Carlo Simulation for Patient Dose Estimation for Examinations With a Cone-Beam 320-MDCT Scanner

Maria Cros[1]
Jacob Geleijns[2]
Raoul M. S. Joemai[2]
Marçal Salvadó[1]

OBJECTIVE. The purpose of this study was to estimate the patient dose from perfusion CT examinations of the brain, lung tumors, and the liver on a cone-beam 320-MDCT scanner using a Monte Carlo simulation and the recommendations of the International Commission on Radiological Protection (ICRP).

MATERIALS AND METHODS. A Monte Carlo simulation based on the Electron Gamma Shower Version 4 package code was used to calculate organ doses and the effective dose in the reference computational phantoms for an adult man and adult woman as published by the ICRP. Three perfusion CT acquisition protocols—brain, lung tumor, and liver perfusion—were evaluated. Additionally, dose assessments were performed for the skin and for the eye lens. Conversion factors were obtained to estimate effective doses and organ doses from the volume CT dose index and dose-length product.

RESULTS. The sex-averaged effective doses were approximately 4 mSv for perfusion CT of the brain and were between 23 and 26 mSv for the perfusion CT body protocols. The eye lens dose from the brain perfusion CT examination was approximately 153 mGy. The sex-averaged peak entrance skin dose (ESD) was 255 mGy for the brain perfusion CT studies, 157 mGy for the lung tumor perfusion CT studies, and 172 mGy for the liver perfusion CT studies.

CONCLUSION. The perfusion CT protocols for imaging the brain, lung tumors, and the liver performed on a 320-MDCT scanner yielded patient doses that are safely below the threshold doses for deterministic effects. The eye lens dose, peak ESD, and effective doses can be estimated for other clinical perfusion CT examinations from the conversion factors that were derived in this study.

Keywords: cone-beam 320-MDCT scanner, International Commission on Radiological Protection (ICRP) computational phantoms, Monte Carlo simulation, patient dose assessment, perfusion CT

DOI:10.2214/AJR.15.14913

Received April 27, 2015; accepted after revision July 21, 2015.

[1]Medical Physics Unit, Faculty of Medicine and Health Sciences, Universitat Rovira i Virgili, C/Sant Llorenç 21, 43201 Reus, Tarragona, Spain. Address correspondence to M. Cros (maria.cros@urv.cat).

[2]Department of Radiology, Leiden University Medical Center, Leiden, The Netherlands.

AJR 2016; 206:129–135

0361–803X/16/2061–129

There is a growing interest in the use of perfusion CT of a wide variety of organs for either research or clinical applications; however, there is also growing concern with regard to radiation exposure of patients from CT in general and from perfusion CT studies in particular [1]. This study addresses the radiation exposure from perfusion CT studies of the brain, lung, and liver with a volumetric 320-MDCT scanner and a 160-mm-wide cone beam.

During perfusion CT studies, IV administration of iodine is performed. Perfusion CT studies require repeated acquisitions of the volume of interest during the first pass of the contrast material, lasting approximately 1 minute, but may also include delayed phases, lasting from 2 to 10 minutes. The dynamic perfusion CT study thus involves a series of continuous or intermittent acquisitions for which the timing of each acquisition, the tube voltage, the tube current, and the rotation time are optimized to achieve the required quality of the study with an optimized radiation exposure of the patient. Various models are being used to derive quantitative information from perfusion CT studies, such as deconvolution or maximum-slope models. Functional hemodynamic parameters, such as blood flow, blood volume, mean transit time, and time to peak enhancement, can be derived from perfusion CT studies.

Particular advantages of perfusion CT are that CT scanners are available for acute patients both during and after working hours and that the perfusion CT examinations are relatively easy to perform. Moreover, perfusion CT results are well suited for quantitative analysis because the voxel values are expressed as Hounsfield units that are related to the linear attenuation coefficient of the tissue, which is sensitive to the concentration of iodine.

The primary application of perfusion CT of the brain is for the diagnosis and assess-

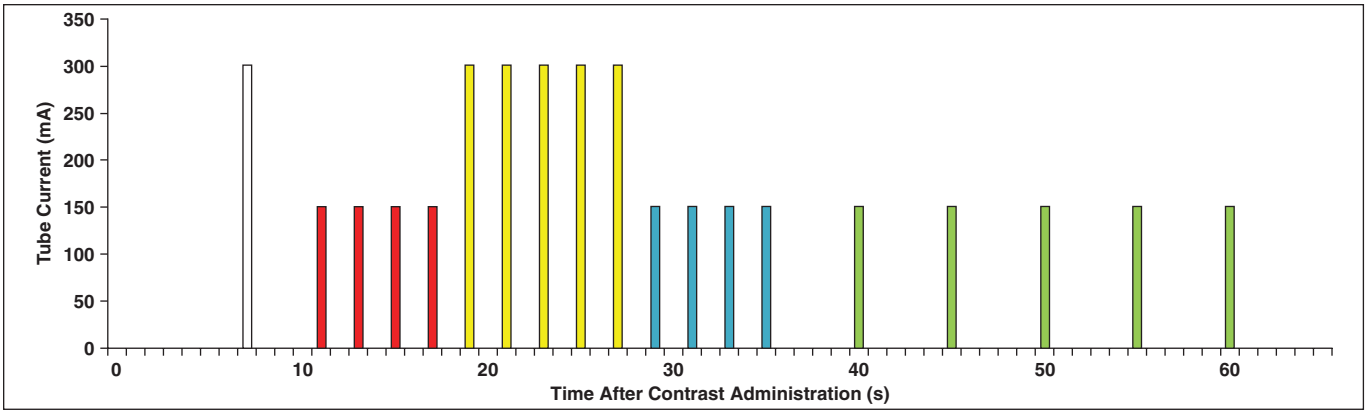

Fig. 1—Bar graph shows tube current values for dynamic acquisition sequences performed for brain perfusion CT examinations. White = mask, red = early arterial phase, yellow = peak arterial phase, blue = late arterial phase, green = venous phase.

ment of stroke [2]. Since the introduction of dynamic volumetric CT of the entire brain, this use of perfusion CT has become a relatively common clinical application. For perfusion CT of the body, the primary application is in oncology—for example, for lesion characterization and for assessment of tumor response to medication or radiation [3, 4]. Perfusion CT studies are still performed primarily as research applications.

Radiation protection in perfusion CT studies is particularly relevant because patient dose rises substantially during the dynamic study when the volume of interest is scanned repeatedly. In perfusion CT studies, it is of interest to assess organ dose and effective dose. With the recent insight that the eye lens is sensitive for radiation-induced cataract [5], it is also of importance to assess the dose to the eye lens during perfusion CT of the brain. It is also necessary to assess the peak entrance skin dose (ESD) accurately for perfusion CT acquisitions because the threshold dose for induction of deterministic skin effects is relatively low, and the skin dose accumulates significantly during the study. The sensitivity of skin is different at different body parts. The mildest deterministic effect that will be observed for the skin of the skull is epilation, but for the body, the mildest effect is skin erythema [6]. Deterministic skin effects are not expected at a peak ESD of less than 2000 mGy. In the past, incorrectly designed acquisition protocols caused an excessively high skin dose for perfusion CT studies of the brain and led to epilation of the skin in certain patients [7]; these cases stress the importance of assessment of skin dose for perfusion CT studies [7].

Patient dosimetry in perfusion CT studies should be performed according to the latest international standards. This requirement means that the effective dose should be calculated according to the latest definitions of the International Commission on Radiological Protection (ICRP) [8]. Moreover, the ICRP has recently published voxel models for the standard adult man and standard adult woman that realistically reproduce human anatomy for dose assessments [9]. Dose assessments for these voxel phantoms can be performed with Monte Carlo simulations.

The purpose of this study was to evaluate patient dose for clinical perfusion CT protocols for imaging the body and the brain. The dosimetric characteristics of the volumetric scanner that was used for the perfusion CT examinations in this study (Aquilion ONE, Toshiba Medical Systems) were modeled in an algorithm for Monte Carlo simulations, and the two ICRP voxel phantoms were included in these simulations. Organ dose (including dose to the eye lens), effective dose, and ESD were assessed. The results are correlated with well-established standards in CT dosimetry, the volume CT dose index ($CTDI_{vol}$), and dose-length product (DLP) to determine the corresponding conversion factors.

Materials and Methods

Monte Carlo Simulation

A Monte Carlo simulation–based code was used to perform the simulations. The program was developed and validated for a cone-beam 320-MDCT scanner (Aquilion ONE) in a previous study [10]. For the calculation of radiation transport, the Electron Gamma Shower Version 4 (EGS4) package (Stanford Linear Accelerator Center) [11] in combination with low-energy photon scattering expansion (National Laboratory for High Energy Physics) [12] was used. The developed Monte Carlo tool takes into account all aspects that have an effect on dose during a CT study, such as x-ray spectrum, x-ray collimation characteristics (including the penumbra), bowtie filtration (related to field size), and heel effect. Additionally, CT acquisition protocol parameters, such as tube voltage, tube current, pitch, tube position, and scanning range, are introduced as inputs. According to the given parameters, the program calculates the absorbed energy in each voxel of the volume, and 3D dose distributions are generated.

The Monte Carlo simulations were performed at a supercomputing center and were performed using 20×10^6 photon histories. The computation time for one acquisition—that is, one full rotation for a volumetric acquisition—was 20 minutes on average.

Voxel Phantoms

The adult reference computational phantoms for an adult man and an adult woman published by the ICRP [9] were used in this study. These phantoms were constructed from CT images of patients and represent an average adult man (average height, 178 cm; average weight, 73 kg) and an average adult woman (average height, 168 cm; average weight, 60 kg). The voxel size is $2.137 \times 2.137 \times 8.000$ mm^3 for the male phantom and $1.775 \times 1.775 \times 4.840$ mm^3 for the female phantom. The implementation of adult male and adult female phantoms in the simulation program was performed using the information (mass, spatial distribution, and composition) of each organ or tissue provided in an ICRP report [9]. Each voxel phantom was implemented as three different representations: one concerning the 53 materials to define their chemical properties used during the radiation transport, one to classify the 141 organs or tissues, and one to label the 29 organs that contribute to the effective dose calculation. This type of classification is useful to calculate the dose of each organ or tissue when the simulation is finished. Because microscopic structures of the skeleton are smaller

than the size of a voxel, a specific subsegmentation was implemented for tissues containing red bone marrow or endosteum (bone surface). In addition, the energy of the secondary particles released from mineral bone components was taken into account through an enhancement factor.

Perfusion CT Acquisition Protocols

The Monte Carlo simulations were performed using three different perfusion CT acquisition protocols: brain, lung tumor, and liver. The parameters for the three protocols are provided in Table 1. In the brain perfusion CT protocol, a series of intermittent volume scans were obtained over a 60-second period. The first volume was used as the mask for dynamic subtraction, and the next series are performed every 2 seconds during the arterial phase (early arterial, peak arterial, and late arterial); the tube current was increased in the peak arterial phase to ensure that the appropriate image quality was achieved. The last series acquires volumes every 5 seconds to capture the slower venous flow. Figure 1 shows a schematic representation of the dynamic acquisition sequence for the brain perfusion CT protocol.

All of the acquisitions were obtained as axial volumetric scans with a nominal beam width of 160 mm. The nominal scanning length was 160 mm in all cases, and the actual exposed length was 170 mm, considering overbeaming. The arms of the phantoms were removed for the lung tumor and liver perfusion CT protocols, thus taking into account that the arms are not positioned alongside the body but are positioned above the head during these clinical perfusion CT examinations.

The lung tumor perfusion CT protocol is performed with 40–60 mL of IV contrast medium administered at a flow rate of 5–7 mL/s, the liver perfusion CT protocol is performed with 30–80 mL of contrast medium administered at a flow rate of 6–10 mL/s, and the brain perfusion CT protocol is performed with 50 mL of contrast medium administered at a flow rate of 5–6 mL/s depending on patient weight. All the protocols are performed with a contrast medium with a concentration of 370 mg I/mL.

TABLE 1: Acquisition Parameters for the Three Perfusion CT Examinations According to the Manufacturer's Recommendations[a]

Perfusion CT Examinations	Peak Tube Voltage (kVp)	Rotation Time (s)	Tube Current (mA)	No. of Scans	Total Tube Current–Exposure Time Product (mAs)	FOV
Brain						
Mask	80	0.75	300	1	225	S
Early arterial phase	80	0.75	150	4	450	S
Peak arterial phase	80	0.75	300	5	1125	S
Late arterial phase	80	0.75	150	4	450	S
Venous phase	80	0.75	150	5	562.5	S
Lung tumor	100	0.5	60	36	1080	M
Liver	100	0.5	100	23	1150	L

Note—S = small bow-tie filter, M = medium bow-tie filter, L = large bow-tie filter.
[a]Aquilion ONE, Toshiba Medical Systems.

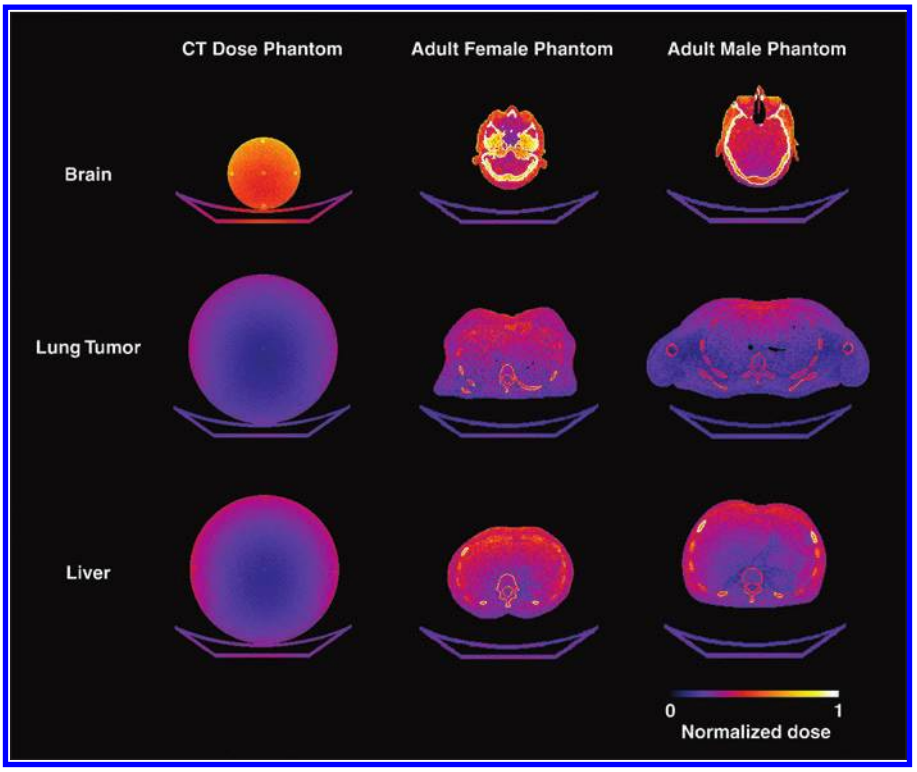

Fig. 2—Normalized dose distributions in CT dose phantom (*left*), adult female phantom (*middle*), and adult male phantom (*right*) for brain perfusion CT examinations (*top row*), lung tumor perfusion CT examinations (*middle row*), and liver perfusion CT examinations (*bottom row*).

Dose Calculations

Monte Carlo simulations using the acquisition parameters shown in Table 1 for the three perfusion CT protocols were performed with two standard CT dose phantoms (150 mm-long; head phantom: 160 mm diameter; body phantom: 320 mm diameter) using a 100-mm-long CT ionization chamber and following the same methods used in previous studies [10, 13]. The $CTDI_{vol}$ values were obtained from the simulations for each perfusion CT study, which corresponds to the average dose in the 100-cm-long CT ionizing chamber according to the definition published by the International Electrotechnical Commission [14]. The results were compared with the $CTDI_{vol}$ value that appeared in the console of the Aquilion ONE scanner for each perfusion CT protocol. The differences between the results and the values on the console were approximately 1%.

The mean absorbed dose in each organ or tissue was computed as the total absorbed energy in the voxels corresponding to the organ or tissue divided by the total mass. Sex-specific calculations of effective doses were performed using the tissue-weighting factors from ICRP Report 103 [8] for each protocol. Additionally, sex-averaged effective doses were calculated considering a tissue-weighting factor of 0.24 for breast tissue of the adult female phantom and no tissue-weighting factor for breast of the adult male phantom. These averaged effective dose results were also normalized to the total tube charge (i.e.,

TABLE 2: Dose-Length Product (DLP), Effective Dose, and Conversion Factors for Estimating Effective Dose From DLP for the Three Perfusion CT Examinations

Perfusion CT Examinations	DLP (mGy × cm)	Effective Dose (mSv)			Sex-Averaged Effective Dose Normalized to Total Tube Current–Exposure Time Product ($\times 10^{-3}$ mSv/mAs)	Conversion Factors for Estimating Effective Dose From DLP ($\times 10^{-3}$ mSv/mGy × cm)
		Adult Male Phantom	Adult Female Phantom	Sex-Averaged		
Brain	3016	3.5	4.6	4.1	1.5	1.4
Lung tumor	995	17.0	25.0	23.4	21.7	23.5
Liver	1175	27.3	26.3	25.7	22.3	21.9

total tube current–exposure time product). For each protocol, the DLP was derived from the $CTDI_{vol}$ obtained from the simulations with the CT dose phantoms and taking into account the nominal scanning length. Additionally, conversion factors for estimating the effective dose from DLP were calculated.

Eye Lens Dose and Peak Entrance Skin Dose Estimations

Although not required for the effective dose calculation, the absorbed dose of the eye lens in the adult male phantom and adult female phantom was reported for the brain perfusion CT protocol. Moreover, the sex-averaged eye lens dose was calculated. For the peak ESD estimation, dose distributions in voxels identified as skin were generated for each protocol (brain, lung tumor, and liver). The peak ESD was computed by selecting the region with the highest value of absorbed dose and by averaging the dose values of the voxels in this region equivalent to 1 cm^2 of skin surface. The sex-averaged peak ESD was calculated. Conversion factors to estimate the eye lens dose and the peak ESD from $CTDI_{vol}$ were also obtained.

Results

The Monte Carlo program used to perform the simulations, which reproduce accurately the dosimetric characteristics of the Aquilion ONE scanner, enabled the dose assessments in the ICRP voxel phantoms (adult male and adult female phantoms) for the perfusion CT brain, lung tumor, and liver acquisitions.

Figure 2 shows the normalized dose distributions of one axial section in three phantoms—the CT dose phantom, the adult male phantom, and the adult female phantom—for the three perfusion CT protocols. The regions with the highest absorbed dose can be identified, such as the skeleton for all perfusion CT acquisitions. Absorbed doses for the adult male and adult female phantoms are presented in Figure 3 for the three perfusion CT protocols. Selection was based on either an exceeded limit of 10 mGy or a total percentage contribution to the effective dose of greater than 90%. The corresponding $CTDI_{vol}$ is indicated for comparison with the organ doses.

Table 2 shows the DLPs and the effective doses for the brain, lung tumor, and liver perfusion CT protocols. Effective doses are presented separately for adult male and adult female phantoms and are also sex-averaged and normalized to the total tube charge. The DLP-to–effective dose conversion factors are also shown for the three perfusion CT acquisitions. For the brain perfusion CT protocol, the total effective dose was computed by the sum of the contribution of the five series performed with different acquisition parameters (Fig. 4).

The eye lens dose for the brain perfusion CT protocol and the peak ESD for all perfusion CT studies are presented in Table 3 and are compared with the $CTDI_{vol}$ values. The absorbed dose distribution in the voxels identified as skin in the adult female phantom derived from a brain perfusion CT acquisition is presented as a cumulative dose–volume histogram (Fig. 5). This histogram relates radiation dose, which is represented along the horizontal axis, to the volume of skin receiving radiation greater than or equal to the corresponding dose.

Discussion

This study used a Monte Carlo simulation tool to estimate the radiation dose from brain, lung tumor, and liver perfusion CT protocols using the adult male and adult female voxel phantoms from the ICRP and a cone-beam 320-MDCT scanner. Conversion factors were obtained to estimate effective doses from values that are indicated on the scanner console, such as $CTDI_{vol}$ and DLP. Moreover, dose assessment was performed for the skin and eye lens.

Dose distributions in the three phantoms used (CT dose phantom, adult male phantom, and adult female phantom) can be compared using the calculation of the average dose volume. The average dose volume, computed as the total energy in the directly irradiated volume divided by the total mass in the same volume and averaged for male and female phantoms, was 182.8 mGy for brain perfusion CT studies and 58.7 and 73.6 mGy for lung tumor and liver perfusion CT studies, respectively. These results were close to the corresponding $CTDI_{vol}$, representing 97%, 94%, and 100% of the respective $CTDI_{vol}$ values.

A similar relationship can be observed in Figure 3. The organ doses were higher for

TABLE 3: Eye Lens Dose for Brain Perfusion CT and Peak Entrance Skin Dose (ESD) for the Three Perfusion CT Examinations

Perfusion CT Examination	$CTDI_{vol}$ (mGy)	Eye Lens				Peak ESD	
		Absorbed Dose (mGy)			% of $CTDI_{vol}$	Sex-Averaged Absorbed Dose (mGy)	% of $CTDI_{vol}$
		Adult Male Phantom	Adult Female Phantom	Sex-Averaged			
Brain	188.5	168.1	137.7	152.9	81.1	255	135
Lung tumor	62.3					157	252
Liver	73.6					172	234

Note—$CTDI_{vol}$ = volume CT dose index.

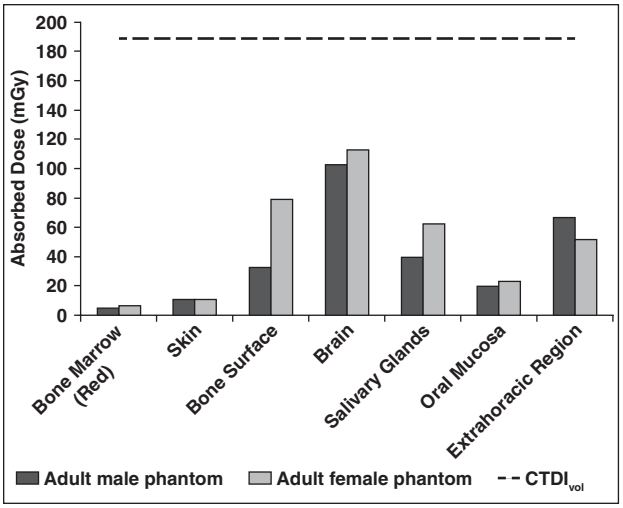

A

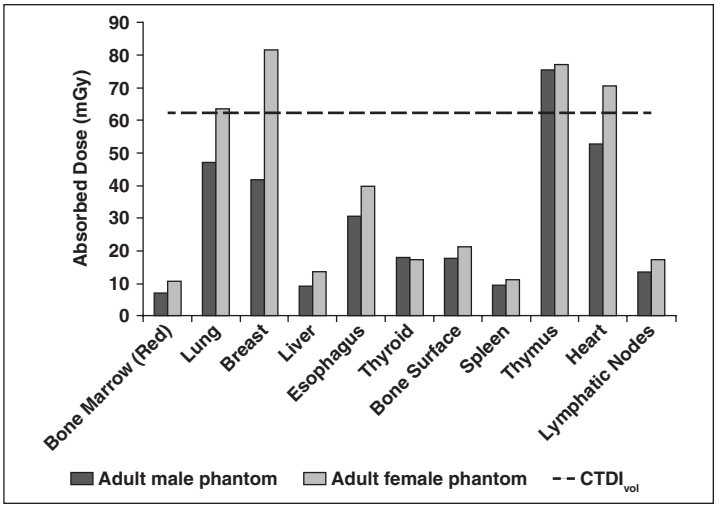

B

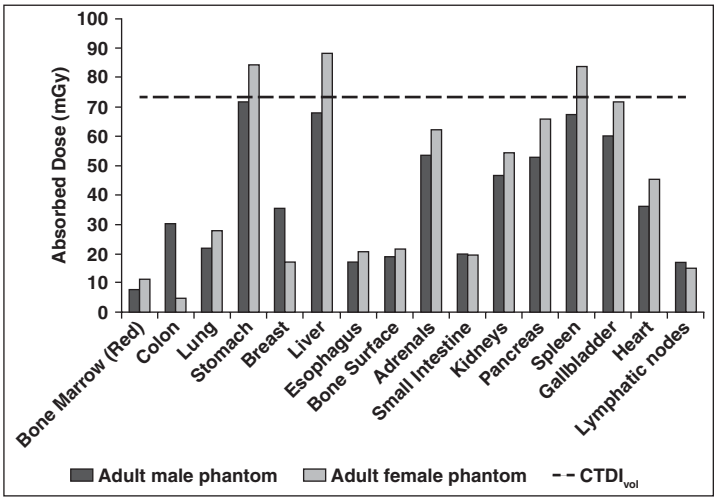

C

Fig. 3—Absorbed doses for adult male phantom and adult female phantom in three perfusion CT protocols. Volume CT dose index ($CTDI_{vol}$) is also indicated.
A–C, Results for brain (**A**), lung tumor (**B**), and liver (**C**) perfusion CT protocols are shown.

brain perfusion CT examinations than for body perfusion CT examinations. For brain perfusion studies, the most relevant value was the absorbed dose in the brain because it is contained within the directly irradiated region, whereas the other organs were partially irradiated. For body perfusion CT studies, the organs within the direct beam received doses that were close to the $CTDI_{vol}$. Figure 3 shows the comparison between the $CTDI_{vol}$ value and the organ doses in the adult male and adult female phantoms from which the relation between organ doses and $CTDI_{vol}$ can be derived. The organs with the highest absorbed doses were lung, breast, thymus, and heart for the lung tumor perfusion CT protocol and the stomach, liver, and spleen for the liver perfusion CT protocol, in which the partially irradiated organs, such as adrenals, kidneys, pancreas, and gallbladder, also received a substantial absorbed dose.

Several relevant differences between organ doses in the adult male and adult female phantoms can be observed. For the brain perfusion CT protocol, the quotient between bone surface dose in the adult female phantom and adult male phantom was 2.4. These differences can be explained because bone surface mass in men is twice the mass in women and the absorbed energy in women is 30% higher than in men. For the perfusion CT liver examinations, doses in the colon and breast in the adult male phantom were higher than these organ doses in the adult female phantom. This difference can be explained because the directly irradiated volume proportions of colon and breast are larger in the adult male phantom than in the adult female phantom: 69.3% of the breast volume is irradiated in the adult male phantom and 11.0% in the adult female phantom and 44.7% of the colon volume is irradiated in the adult male phantom and 0.5% in the adult female phantom.

The sex-averaged effective doses from the brain perfusion CT studies were approximately 4 mSv. As can be observed in Figure 4, the maximum contribution was from the peak arterial series because of the total tube current used in it. The effective dose for the adult female phantom was higher than that for the adult male phantom for all five series, even though a proportional contribution can be observed in each series of the protocol. For the lung tumor and liver perfusion CT studies, the sex-averaged effective doses were 5.8 and 6.3 times higher than the effective dose from the brain perfusion CT studies, respectively. For the liver examinations, the effective dose in the adult male phantom was slightly higher than that in the adult female phantom because of the large contribution of colon and breast organ doses. In this case, because no tissue-weighting factor for breast in adult men was used, the sex-averaged effective dose was lower than the same sex-specific values.

The DLPs for the liver and lung tumor examinations were of the order of magnitude of 1000 mGy × cm, whereas for the brain examinations, the DLP was 3 times higher. These results reflect the differences in the total tube current used in the brain perfusion CT studies compared with the body perfusion CT studies. Additionally, these values are influenced by the size differences (i.e., attenuation differences) between the head and the body of the phantoms.

The effective doses obtained in this study are consistent with the results reported by other authors (3.6 mSv) for a similar brain perfusion CT protocol on a 320-MDCT scanner using thermoluminescent dosimeters (TLDs) in a Rando phantom (The Phan-

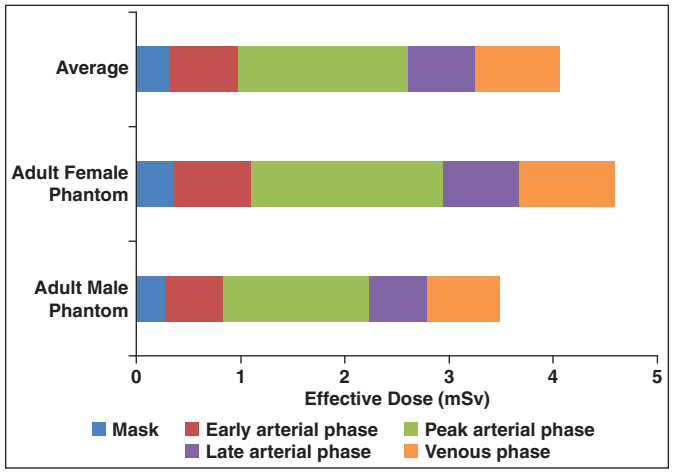

Fig. 4—Schematic shows contribution to effective dose of each series in brain perfusion CT protocol.

tom Laboratory) [15]. Other studies use k factors, obtained from 64-MDCT scanners [16, 17], to quantify the effective dose associated with head or body perfusion 320-MDCT protocols. In comparison with the results of the current study, these k factors overestimated the effective dose by approximately 63% in the brain perfusion CT protocol and underestimated it by approximately 34% in the body perfusion CT acquisitions. To our knowledge, studies on effective doses for body perfusion CT protocols using simulations or measurements in anthropomorphic phantoms have not been published.

The sex-averaged eye lens dose from the brain perfusion CT examinations was approximately 153 mGy, which is 81% of the $CTDI_{vol}$. The eye lens dose in the adult female phantom was lower than that in the adult male phantom due to the position of the eyes in the head. The fraction of bone in the same slice of eye lens in the adult female phantom is larger than that in the adult male phantom, leading to a higher attenuation of radiation in the adult female phantom. The organ doses do not exceed the thresholds suggested by ICRP guidelines for the deterministic effects in the lens of the eyes [18]. The lowest threshold is 500 mGy for a posterior subcapsular cataract with a period of latency of 8 years. Because sensitivity to radiation can differ depending on patient age and patient disease, eye lens dose must be taken into account on a patient-by-patient basis. Moreover, radiation can accelerate cataracts caused by other factors (e.g., ultraviolet B radiation, diabetes, corticosteroid use). The results from the current study are higher than those published by other authors for similar brain protocols with a volumetric 320-MDCT scanner but using TLD measurements in a Rando phantom [15]. This discrepancy in results can be explained by the differences in the phantoms used.

Although skin doses were on the order of magnitude of 10 mGy in the three perfusion CT studies, the peak ESDs in the directly irradiated region were more relevant and must be evaluated. The thresholds in a single brief exposure for early transient erythema and temporary epilation are 2000 and 3000 mGy, respectively [18]. These values represent a dose average for the entire population; as a consequence, possible variations in patients must be considered. The sensitivity to radiation differs depending on factors such as the dose rate or the irradiated area; for example, the skin of the head is more resistant to radiation than the irradiated skin in a lung examination. However, in the current study, the peak ESD was 255 mGy for the brain perfusion CT protocol, 157 mGy for the lung tumor perfusion CT studies, and 172 mGy for the liver perfusion CT studies. Thus, the maximum ESDs from brain, lung tumor, and liver perfusion CT studies in an Aquilion ONE unit were lower than these thresholds, representing 8–13% of the lowest dose threshold.

Conversion factors to estimate the peak ESD from $CTDI_{vol}$ for the three perfusion CT protocols were provided from the data provided in Table 3. These values, which can be a useful tool in clinical practice, were 1.4, 2.5, and 2.3 mSv/mGy for the brain, lung tumor, and liver perfusion CT protocols, respectively.

In the case of a brain perfusion CT examination, which presents higher skin doses, Figure 5 shows a detailed analysis of the dose in all the voxels identified as skin in an adult female phantom. The percentage of skin voxels that received each absorbed dose (presented in milligrays) can be read from the skin dose–volume histogram: 16% of the skin voxels received some part of the dose, from which approximately 60% received doses lower than 110 mGy. From the dose distribution map, voxels with values greater than 110 mGy were identified as those that are directly irradiated. The noncumulative dose–volume histogram in the directly irradiated area corresponds to a gaussian function, where the maximum is 192 mGy (mean dose in voxels within the scanning area). This mean skin dose corresponds to 75% of the peak ESD, but it is closer to the $CTDI_{vol}$. The results presented in this study were higher than those published by other authors for a 320-MDCT scanner [15]; in that study, the authors measured skin dose in a scanned area (92 mGy) using a located TLD's measurement, but they were not able to determine the peak ESD [15].

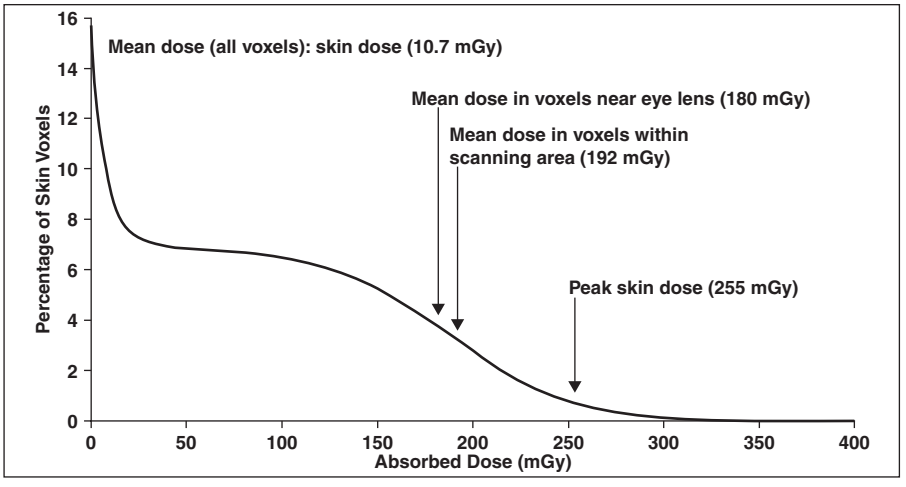

Fig. 5—Cumulative dose-volume histogram for skin derived from brain perfusion CT examination of adult female phantom. Normalized number of voxels for each absorbed dose value (in milligrays) is shown.

In clinical practice, the results of the current study can be useful to estimate dose for patients from the data shown in the console of the Aquilion ONE unit. However, a limitation is that this study focuses on "standard" adult patients. Because the sizes of adult heads have small individual differences, the results obtained for the brain perfusion CT studies can be a good estimation of patient doses. For the body perfusion CT studies, size changes significantly depending on the patient. Thus, the effect of patient size on dose from body perfusion CT protocols needs to be analyzed in future studies.

The radiation dose from perfusion CT studies must be controlled to establish efficient, optimized, and safe protocols without losing relevant diagnostic imaging information. In this study, a Monte Carlo method was used to estimate organ and effective doses from perfusion CT studies of the brain, lung tumors, and liver using a 320-MDCT scanner and computational phantoms from the ICRP. The dose assessments in the eye lens and skin showed that thresholds for deterministic effects were not exceeded in the studied protocols. Clinically, the results presented in this study can be used to estimate eye lens dose, peak ESD, and effective doses from the data ($CTDI_{vol}$ and DLP) that appear in the console of a 320-MDCT scanner (Aquilion ONE) and to ensure that the established protocol is operating below the deterministic effects dose limits.

In conclusion, although $CTDI_{vol}$ is a good conservative estimator of organ doses in the directly irradiated area in a brain perfusion CT examination, including eye lens dose, $CTDI_{vol}$ underestimates several organ doses in body perfusion CT studies. The results indicate that contrary to the eye lens doses, $CTDI_{vol}$ underestimates the peak ESD in all the body perfusion CT examinations. Therefore, the skin dose conversion factors can be useful to estimate peak ESD to optimize the protocols to avoid radiation skin injuries.

References

1. Brix G, Lechel U, Nekolla E, Griebel J, Becker C. Radiation protection issues in dynamic contrast-enhanced (perfusion) computed tomography. *Eur J Radiol* 2014 Nov 20 [Epub ahead of print]
2. Dababneh H, Bashir A, Guerrero WR, et al. Mean transit time on Aquilion ONE and its utilization in patients undergoing acute stroke intervention. *J Vasc Interv Neurol* 2014; 7:73–81
3. Kim SH, Kamaya A, Willmann JK. CT perfusion of the liver: principles and applications in oncology. *Radiology* 2014; 272:322–344
4. Li XS, Fan HX, Fang H, Huang H, Song YL, Zhou CW. Value of whole-tumor dual-input perfusion CT in predicting the effect of multiarterial infusion chemotherapy on advanced non-small cell lung cancer. *AJR* 2014; 203:(web)W497–W505
5. International Commission on Radiological Protection. Statement on tissue reactions. Ottawa, ON, Canada: ICRP, 2011: report no. 4825-3093-1464
6. Geleijns J, Wondergem J. X-ray imaging and the skin: radiation biology, patient dosimetry and observed effects. *Radiat Prot Dosimetry* 2005; 114:121–125
7. Imanishi Y, Fukui A, Niimi H, et al. Radiation-induced temporary hair loss as a radiation damage only occurring in patients who had the combination of MDCT and DSA. *Eur Radiol* 2005; 15:41–46
8. [No authors listed]. The 2007 recommendations of the International Commission on Radiological Protection: ICRP publication 103. *Ann ICRP* 2007; 37:1–332
9. Menzel HG, Clement C, DeLuca P. ICRP publication 110: realistic reference phantoms: an ICRP/ICRU joint effort—a report of adult reference computational phantoms. *Ann ICRP* 2009; 39:1–164
10. Salvadó M, Cros M, Joemai RMS, Calzado A, Geleijns J. Monte Carlo simulation of the dose distribution of ICRP adult reference computational phantoms for acquisitions with a 320 detector-row cone-beam CT scanner. *Phys Med* 2015; 31:452–462
11. Nelson WR, Hirayama H, Rogers DW. The EGS4 code system. Stanford, CA: Stanford Linear Accelerator Center, 1985: report SLAC-265
12. Hirayama H, Namito Y, Ban S. Implementation of a general treatment of photoelectric-related phenomena for compounds or mixtures in EGS4: KEK internal report 2000-3. National Laboratory for High Energy Physics rcwww.kek.jp/research/egs/kek/egs4/photo.pdf. Published May 2000. Accessed July 15, 2015
13. Geleijns J, Salvadó Artells M, de Bruin PW, Matter R, Muramatsu Y, McNitt-Gray MF. Computed tomography dose assessment for a 160 mm wide, 320 detector row, cone beam CT scanner. *Phys Med Biol* 2009; 54:3141–3159
14. International Electrotechnical Commission. Medical electrical equipment: part 2-44—particular requirements for the basic safety and essential performance of x-ray equipment for computed tomography. Geneva, Switzerland: IEC, 2009: report no. IEC 60601-2-44-ed30
15. Diekmann S, Siebert E, Juran R, et al. Dose exposure of patients undergoing comprehensive stroke imaging by multidetector-row CT: comparison of 320-detector row and 64-detector row CT scanners. *AJNR* 2010; 31:1003–1009
16. Bongartz G, Golding SJ, Jurik AG, et al. European Guidelines on Quality Criteria for Computed Tomography Luxembourg: European Commission; 2000:EUR 16262
17. Valentin J; International Commission on Radiological Protection. Managing patient dose in multi-detector computed tomography (MDCT): ICRP publication 102. *Ann ICRP* 2007; 37:1–79, iii
18. Stewart FA, Akleyev AV, Hauer-Jensen M, et al. ICRP publication 118: ICRP statement on tissue reactions and early and late effects of radiation in normal tissues and organs—threshold doses for tissue reactions in a radiation protection context. *Ann ICRP* 2012; 41:1–322